ARL-TN-1264 ● JULY 2025

Survey of Silicon Carbide Interatomic Potentials

by Matthew Guziewski and Shawn P. Coleman

NOTICES

Disclaimers

The findings in this report are not to be construed as an official Department of the Army position unless so designated by other authorized documents.

Citation of manufacturer's or trade names does not constitute an official endorsement or approval of the use thereof.

Destroy this report when it is no longer needed. Do not return it to the originator.

ARL-TN-1264 ● JULY 2025

Survey of Silicon Carbide Interatomic Potentials

Matthew Guziewski and Shawn P. Coleman
DEVCOM Army Research Laboratory

REPORT DOCUMENTATION PAGE

1. REPORT DATE	2. REPORT TYPE	3. DATES COVERED	
		START DATE	END DATE
July 2025	Technical Note	01 October 2019	30 September 2021

4. TITLE AND SUBTITLE
Survey of Silicon Carbide Interatomic Potentials

5a. CONTRACT NUMBER	5b. GRANT NUMBER	5c. PROGRAM ELEMENT NUMBER
5d. PROJECT NUMBER 611102.AA7.03	**5e. TASK NUMBER**	**5f. WORK UNIT NUMBER**

6. AUTHOR(S)
Matthew Guziewski and Shawn P. Coleman

7. PERFORMING ORGANIZATION NAME(S) AND ADDRESS(ES)	8. PERFORMING ORGANIZATION REPORT NUMBER
DEVCOM Army Research Laboratory ATTN: FCDD-RLA-ME Aberdeen Proving Ground, MD 21005	ARL-TN-1264

9. SPONSORING/MONITORING AGENCY NAME(S) AND ADDRESS(ES)	10. SPONSOR/MONITOR'S ACRONYM(S)	11. SPONSOR/MONITOR'S REPORT NUMBER(S)

12. DISTRIBUTION/AVAILABILITY STATEMENT
DISTRIBUTION STATEMENT A. Approved for public release: distribution unlimited.

13. SUPPLEMENTARY NOTES
ORCIDs: Matthew Guziewski, 0000-0002-5761-720X; Shawn P. Coleman, 0000-0002-5542-3161

14. ABSTRACT
This technical note is an overview of the work performed to determine viable potentials for a molecular dynamics (MD) study of silicon carbide grain boundaries and other phase boundaries within the silicon-carbon (material system. Because MD simulations are only as accurate as the interatomic potential used, a robust study of how well each potential models relevant properties is necessary. This work compares MD results with both experimental and density functional theory values to validate the use of a particular potential (or potentials) to study this complex material system.

15. SUBJECT TERMS
Sciences of Extreme Materials, molecular dynamics, MD, silicon carbide, SiC, interatomic potentials, grain boundaries

16. SECURITY CLASSIFICATION OF:			17. LIMITATION OF ABSTRACT	18. NUMBER OF PAGES
a. REPORT	b. ABSTRACT	C. THIS PAGE		
UNCLASSIFIED	UNCLASSIFIED	UNCLASSIFIED	UU	27

19a. NAME OF RESPONSIBLE PERSON	19b. PHONE NUMBER *(Include area code)*
Matthew Guziewski	(520) 691-5019

STANDARD FORM 298 (REV. 5/2020)
Prescribed by ANSI Std. Z39.18

Contents

List of Figures

List of Tables

1. Interatomic Potentials Considered

Below is a list of the nine interatomic potentials that we considered for use in this study. All work was performed using the Large-scale Atomic/Molecular Massively Parallel Simulator (LAMMPS) molecular dynamics (MD) code.[1] Potentials are categorized as follows:

- Tersoff potentials (Tersoff,[2–4] Devanathan et al.,[5] and Erhart and Albe[6])
- Modified embedded-atom method (MEAM) potential (Huang et al.[7])
- Gao–Weber (GW) potentials (Gao and Weber[8] and Belko et al.[9])
- Environment-dependent interatomic potential (EDIP) (Jiang et al.[10])

Two of the Tersoff potentials, Tersoff[2] and Erhart and Albe,[6] have been further adapted using a reactive empirical bond-order (REBO) formulation by Pastewka et al.,[11] which demonstrated better model fracture, brittle behavior, and the amorphous silicon carbide (a-SiC) structure, all of which are relevant to this study. Both formulations of these potentials are shown in this report, with the REBO potential's values given in parenthesis. In addition, a Vashishta et al.[12] style potential was also initially considered; however, because it was incapable of modeling single-element structures of silicon (Si) and carbon (C), the Vashishta et al.[12] potential was deemed unsuitable for this study.

2. Known Si-C Structures

The first step in determining the validity of each potential is to test how well it models the known crystal structures within the SiC system. These include Si, diamond C, graphitic C, and several polytypes of SiC (Figure 1). Values for lattice constants, elastic constants, and cohesive energies were determined and compared with values from literature.

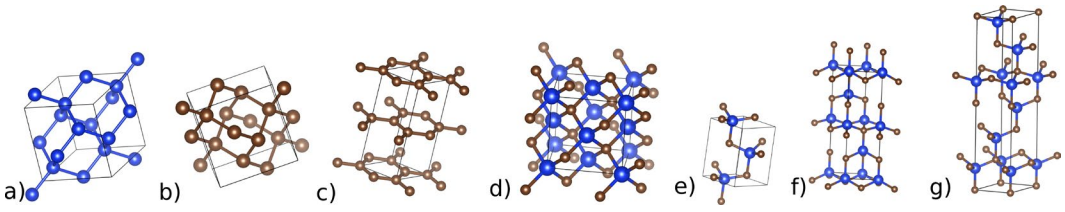

Figure 1. Known crystal structures in the Si (blue) and C (brown) system that were considered in this work. a) Si, b) diamond, c) graphite, d) SiC-C3, e) SiC-H2, f) SiC-H4, and g) SiC-H6.

2.1 Crystal Structure Testing

2.1.1 SiC Polytypes

Table 1 shows all potentials are within 2% of the experimentally observed lattice constants and 3% of the experimentally observed formation energy. Although the experimentally observed elastic constants and those predicted by the potentials have larger variation (on the order of 10%), this is still reasonably accurate for an interatomic potential. However, the GW style potentials are an exception to this because they differed on the scale by a factor of 2. It suggests that this style of potential may not be appropriate for this study, especially regarding mechanical response.

Table 1. Lattice constants (Å), cohesive energy (eV/atom), and elastic constants (GPa) for SiC polytypes using all considered potentials as well as experimentally (Exp) reported values.[13,14]

Reference	2[a]	3	4	5	6[a]	7	8	9	10	Exp
SiC-C3	. . .	. . .	. . .	. . .	. . .	. . .	. . .	. . .	. . .	. . .
a	4.32	4.31	4.28	4.28	4.36	4.36	4.36	4.36	4.36	4.36
E_c	−6.16	−6.21	−6.43	−6.43	−6.34	−6.43	−6.41	−6.41	−6.34	−6.34
C11	436	426	446	447	384	402	265	265	397	390
C12	118	134	138	138	144	115	219	219	140	142
C44	256	209	220	220	240	215	101	101	170	256
SiC-H2, H4, H6	. . .	. . .	. . .	. . .	. . .	. . .	. . .	. . .	. . .	. . .
a	3.06	3.05	3.03	3.03	3.08	3.08	3.08	3.08	3.08	3.08
c[b]	4.99	4.97	4.94	4.94	5.03	5.03	5.03	5.03	5.04	5.02
E_c	−6.16	−6.21	−6.43	−6.43	−6.34	−6.43	−6.41	−6.41	−6.34	−6.34
C11	523	483	506	506	484	467	319	319	436	501
C33	566	510	534	534	544	498	369	369	453	553
C12	96	118	122	122	123	98	218	218	129	111
C13	53	91	94	94	64	68	167	167	112	53
C44	192	167	176	176	160	167	49	49	142	163

[a] Both original and REBO formulations predict the same values.
[b] Listed values are for SiC-H2. H4 and H6 values are two and three times this value, respectively.

2.1.2 Single-Element Structures

Table 2 shows the results of the potential testing for single-element species, and like the SiC structures, all potentials except for the GW styles had very good accuracy. Because the GW potentials again poorly modeled the elastic constants, and here they were also off in the energetics of the single crystals, they are likely unsuitable for this study and will therefore be eliminated from consideration. Graphite is notoriously difficult to model, and, as such, there are larger variations from experimental values for all potentials. However, two Tersoff potentials (Tersoff[2] and Erhart and Albe[6]) and one EDIP (Jiang et al.[10]) modeled graphite well, and they seem to be robust for the SiC system. These potentials also have very

close diamond- and graphite-cohesive energies, suggesting that they may be able to create stable simulations that contain the graphitic region that sometimes occurs at phase boundaries.

Table 2. Lattice constants (Å), cohesive energy (eV/atom), and elastic constants (GPa) for Si and both diamond (dia) and graphitic (gra) C using all considered potentials, as well as experimentally (Exp) reported values.[15–17]

Reference	2[a]	3	4	5	6[a]	7	8	9	10	Exp
Si	. . .	. . .	. . .	. . .	. . .	. . .	. . .	. . .	. . .	. . .
a	5.43	5.43	5.43	5.43	5.43	5.43	5.22	5.22	5.43	5.43
E_c	−4.63	−4.63	−4.63	−4.63	−4.63	−4.63	−2.82	−2.82	−4.65	−4.63
C_{11}	142	142	142	142	169	162	803	803	155	168
C_{12}	75	75	75	75	64	65	781	781	75	65
C_{44}	69	69	69	69	60	73	6	6	59	80
C (dia)	. . .	. . .	. . .	. . .	. . .	. . .	. . .	. . .	. . .	. . .
a	3.57	3.56	3.56	3.56	3.57	3.57	3.86	3.86	3.56	3.57
E_c	−7.36	−7.47	−7.47	−7.47	−7.37	−7.37	−5.72	−5.72	−7.37	−7.34
C_{11}	1073	1007	1007	1008	1088	1080	224	224	1098	1081
C_{12}	101	169	169	173	125	125	155	155	110	125
C_{44}	641	462	462	463	641	571	134	134	495	579
C (gra)	. . .	. . .	. . .	. . .	. . .	. . .	. . .	. . .	. . .	. . .
a	2.53	2.71	2.79	2.79	2.56	3.31	2.75	2.75	2.59	2.46
c	4.20[b]	3.87[c]	3.35[c]	3.35[c]	4.30[b]	3.19[c]	5.00[b]	5.00[b]	4.40[b]	6.70
E_c	−7.39	−5.65	−5.77	−5.77	−7.37	−6.34	−5.32	−5.32	−7.38	−7.37
C_{11}	1987	655	655	657	1722	677	343	343	1088	1080
C_{33}	53	0	0	0	22	2166	0	0	0	37
C_{12}	−314	218	218	220	−14	−102	147	147	−68	180
C_{13}	0	0	0	0	0	−273	0	0	0	15
C_{44}	0	0	0	0	0	0	0	0	0	4

[a] Both original and REBO formulations predict the same values.

[b] Represents minimum c value; all larger c values will have the same cohesive energy.

[c] Minimized only to a graphite-like structure.

2.2 Surface Free Energies

Due to the brittle nature of the ceramic materials considered here, it is important to consider the surface free energy, which is important in the modeling of crack propagation within these materials. Therefore, the surface energy of the common cleavage surfaces in diamond cubic materials, {100}, {110}, and {111}, was determined for Si, diamond C, and SiC-C3 for each potential. For the {111} surface, there are two potential terminating planes, where the primary difference is the distance from the surface plane to the second nearest {111} plane of atoms. Figure 2a shows this second nearest plane is much further away for plane 2 than plane 1. The result of this is more hanging bonds for plane 2, a factor that will affect the energetics. In addition, there are different possible surface chemistries for SiC within the {100} and {111} (Figure 2b), and, as such, energy values were found for

both the Si and C surfaces. Because the diamond cubic system is known to have surface structures that vary from the bulk structure,[18] simulations were ramped from 0 to 200 K and then back down to 0 K, with each ramp taking place over 5 ns, to overcome the energy barrier to these structures. The results of these simulations are listed in Table 3.

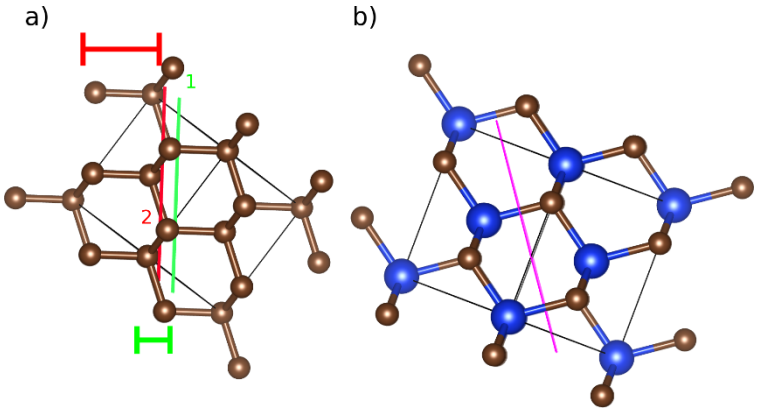

Figure 2. a) Possible terminating {111} planes (green and red) for cubic diamond-structured materials and the distance to second nearest plane. b) Potential surface chemistries for the {111} family of planes in SiC. To the left of the plane (pink) is a surface containing only Si (blue), and to the right is a surface containing only C (brown).

Table 3. Surface energies (J/m^2) of the {100}, {110}, and {111} planes of Si, diamond (dia), and SiC-C3 for all interatomic potentials still under consideration for this study, as well as experimental (Exp) and density functional theory (DFT) values.[11,19,20]

Reference	2 (REBO)	3	4	5	6 (REBO)	7	10	Exp (DFT)
Si	. . .	. . .	. . .	. . .	. . .	. . .	. . .	. . .
γ_{100}	2.25 (6.00)	6.20	2.25	2.25	1.96 (1.30)	2.02	2.06	2.13 (1.53)
γ_{110}	1.51 (4.75)	4.98	1.51	1.51	1.23 (1.23)	1.89	1.21	1.51 (1.68)
γ_{111}	1.19 (4.85)	4.93	1.19	1.19	1.00 (1.00)	1.63	0.97	1.23 (1.72)
C (dia)	. . .	. . .	. . .	. . .	. . .	. . .	. . .	. . .
γ_{100}	6.61 (6.61)	145.9	9.46	9.44	5.57 (5.83)	9.17	5.00	9.2 (5.43)
γ_{110}	4.01 (4.01)	196.5	6.69	6.68	2.94 (2.94)	11.13	1.61	6.5 (5.90)
γ_{111}	2.74 (2.74)	241.4	5.46	5.45	2.06 (2.05)	9.60	1.25	5.3 (6.37)
SiC-C3	. . .	. . .	. . .	. . .	. . .	. . .	. . .	. . .
γ_{100}	3.54 (3.54)	4.88	4.46	4.43	3.38 (3.36)	4.10	2.72	–(3.48)[a]
γ_{110}	2.39 (2.62)	3.49	3.70	3.70	2.26 (2.26)	4.51	1.86	–(3.29)
γ_{111}	1.06 (1.07)	2.66	2.81	2.81	1.66 (1.66)	3.66	1.47	–(4.17)[a]

Note: For SiC-C3, only DFT values were available in literature.
[a] DFT not able to determine energies of different surface chemistries.

For Si, almost all potentials predict surface energies close to those observed experimentally, except for the REBO formulation of the Tersoff[2] potential. However, the facets of diamond are found to be much more difficult to model. Reasonable approximations are made for the surface energy of the {100} plane, with some potentials' prediction energies close to experimental values (Tersoff,[4]

Devanathan et al.,[5] and Huang et al.[7]), whereas others predict values closer to those predicted by DFT (Tersoff,[2] Erhart and Albe,[6] and Jiang et al.[10]). The Tersoff[3] potential predicts energies more than 1 order of magnitude too high, and therefore it is likely not suitable for surface/fracture studies. For the {110} and {111} surfaces of diamond, only two Tersoff potentials (Tersoff[4] and Devanathan et al.[5]) matched experimental and DFT values, with all other potentials predicting energies several J/m^2 too low. Although these values are worth keeping in mind for any fracture/crack growth simulations, fracture in the SiC will likely be much more prevalent, and therefore the variations in diamond from experimental values may be of limited importance. Due to limited literature on the subject, it is difficult to comment extensively on the SiC-C3 surface energies predicted by the potentials. There seems to be an absence of experimental values, and although DFT can predict the surface energy of the {110} plane, due to the structure of SiC and limitations of DFT, the two free surfaces in simulation have different chemistries. As such, the reported DFT values for the {100} and {111} surfaces are an average of the two surface chemistries. For the {110} surface of SiC-C3, the MD results are in reasonable agreement with the DFT results, particularly among the Tersoff potentials (Tersoff,[4] Devanathan et al.,[5] and Erhart and Albe[6]). All potentials also find the {100} surface to have higher energy than the {110}, which is consistent with DFT results, except for Tersoff[2] potential, which finds the Si-terminating surface to have lower energy. This is consistent with experimental observations[21] in which Si is observed at the surface of this cleavage plane. However, there is a discrepancy between the MD and DFT results for the {111} plane of SiC-C3, because all potentials find it to have the lowest surface energy, whereas DFT finds it to have the highest. This phenomenon likely requires further examination, because there are two opposing explanations to this behavior. One possibility is that the second face being sampled in the DFT simulations has a much higher surface energy, and that this is the lowest energy surface, with just the average of these faces being larger. The second possibility is the MD simulations are poorly modeling some surface behavior that the higher-fidelity DFT simulations observe. However, the agreement of all the potentials, which was not the case for both Si and diamond, suggests that it is the former. Except for the MEAM potential (Huang et al.),[7] all potentials exhibit the same trend, $\gamma_{100} > \gamma_{110} > \gamma_{111}$, and, as such, they are all likely suitable for a study of fracture in the SiC-C3.

3. Stable Si-C Structures Validation

Having considered the known structures of the Si-C system, it is also important to check that these potentials do not predict any additional low-energy, stable crystal structures that have not been experimentally observed. The convex hull for the Si-C system consists of only Si, SiC, and graphite. To test the convex hull without bias, an evolutionary algorithm, USPEX,[22] was used to search for potentially low-energy structures. The known structures were seeded into the program, along with 30 randomly generated structures, and run for 50 generations. The structures in each generation were produced from heredity (50%), soft mutation (20%), transmutation (15%), and lattice mutation (5%), and some were created randomly (10%). All the potentials form the proper convex hull shape except for the Tersoff[3] potential (Figure 3), which predicts a stable SiC_5 structure (Figure 4a) that has not been reported experimentally. As such, this potential was eliminated from consideration. Only potentials Tersoff,[2] Erhart and Albe,[6] and Jiang et al.[10] predict graphite to be on the convex hull, with all other potentials having diamond as the lowest energy pure C structure. Of the potentials that correctly predict graphite's presence on the convex hull, all find Si with a C substitutional defect (Figure 4b) to be among the most energetically favorable. This defect has been reported to have a formation energy of 2.3 eV experimentally[23] and 1.69 eV using DFT.[24] All three potentials predict lower-formation energies, 0.97 eV, 0.36 eV, and 0.86 eV for Tersoff,[2] Erhart and Albe,[6] and Jiang et al.[10] potentials, respectively. Although the focus of this study will likely be far from this composition, the low formation energy of the Erhart and Albe[6] Tersoff potential—in particular—is worth keeping in mind.

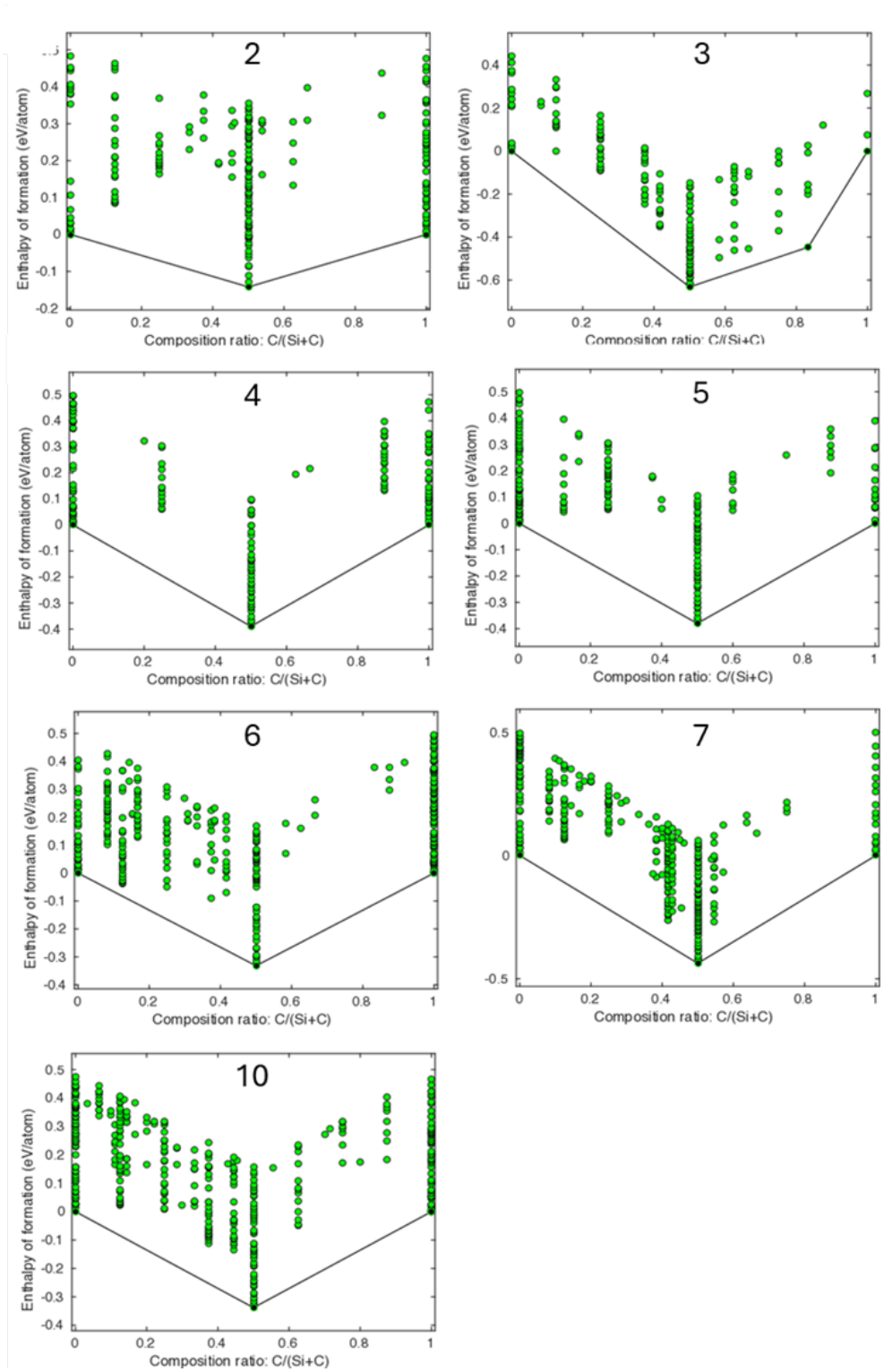

Figure 3. Convex hulls predicted for all the interatomic potentials, numbered by reference, still under consideration by the USPEX evolutionary algorithm. In the Si-C system Si, SiC, and graphite should lie on the convex hull, because they are the only stable structures. The REBO formulations of Tersoff[2] and Erhart and Albe[6] produced almost identical convex hull to those shown.

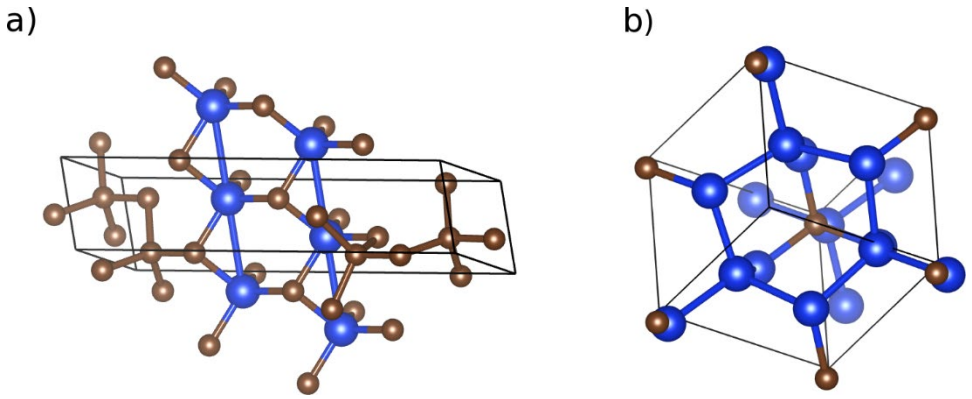

Figure 4. a) SiC_5 crystal structure predicted by Tersoff[3] potential to be stable. b) Si with a C substitutional defect found to be the lowest energy crystal structure not on the convex hull for most of the potentials. Si is shown in blue and C is shown in brown.

One additional potentials elimination was made, because two Tersoff potentials (Tersoff[4] and Devanathan et al.[5]) reported identical values for all tests performed thus far. This is to be expected because the two potentials are almost identical, except that Devanathan et al.[5] also includes the Ziegler–Biersack–Littmark screened nuclear repulsion term that only applies to high-energy collisions between atoms. Therefore, the Tersoff[4] potential was also eliminated from further consideration in the best interest of computational efficiency.

Because there are many high-temperature applications to SiC, it is worthwhile to explore how these interatomic potentials respond to changes in temperature. In addition, knowledge of the thermal expansion and melting points will aid in construction of simulations as the project moves forward. All temperature simulations were performed using a Nosé–Hoover thermostat and Parrinello–Rahmen barostat. The pressure was set to zero, and temperatures were ramped up to 100 K over 10 ns, and then held at the temperature for 5 ns up to a temperature of 6000 K. Time averages were then taken for both the temperature and lattice constants over the 5-ns hold.

All potentials performed reasonably well with changes in temperature, except for the REBO formulation of the Tersoff[2] potential. Due to an instability in this potential, Si expanded rapidly at a relatively low temperature. This made it unsuitable for any temperature studies, so this potential will be removed from any future consideration. Only the EDIP potential (Jiang et al.[10]) produced a melting temperature close to that of experimental values; however, this potential also significantly underpredicts the melting temperature of both diamond and SiC-C3. Although this does not eliminate this potential, care must be taken when using this in MD simulations to ensure no melting is occurring. The thermal expansion predicted by all the potentials was higher than experimentally observed values

(Table 4), but not to a degree that would disqualify any of them from use in simulations.

Table 4. Thermal expansion coefficients, $\alpha \times 10^6$ (K^{-1}), and melting temperatures, T_m (K), predicted by the various interatomic potentials still under consideration, as well as experimental (Exp) values.[25–27]

Reference	2 (REBO)	5	6 (REBO)	7	10	Exp
Si	. . .	. . .	. . .	. . .	. . .	. . .
α	5.34 (−)	3.91	6.25 (7.93)	13.07	0.34	3.05
T_m	3400 (−)	3400	3400 (3000)	3000	1600	1412
C (dia)	. . .	. . .	. . .	. . .	. . .	. . .
α	6.15 (8.46)	5.07	5.90 (8.15)	12.04	4.19	1.06
T_m	4700 (5700)	NA	3700 (5800)	5400	2200	NA
SiC-C3	. . .	. . .	. . .	. . .	. . .	. . .
α	12.49 (9.50)	12.69	10.55 (9.36)	12.89	9.69	4.45
T_m	4400 (4600)	5300	4900 (5100)	4400	2900	4946

Note: dia = diamond; NA = not applicable.

4. SiC Grain Boundaries

To evaluate how well each potential modeled a grain boundary (GB) structure, DFT results from the three Σ5 GB types—the [210] Si-terminated, the [210] C-terminated, and the [310]—were used as initial structures and then minimized with each of the remaining potentials still under consideration. Three simulations were then run for each structure:

1) Minimization of the initial structure used in the DFT simulations to test if the MD results would find the same minimum energy structure.
2) Minimization of the optimized DFT structure to test how much variation in atomic position between DFT and MD there is.
3) Minimization of the optimized DFT structure made 10 times larger in both interface plane directions to determine if there are any size effects not seen in the DFT simulations.

In addition, because both [210] structures do not have an equal number of Si and C atoms, only upper and lower bounds to the interfacial energy could be determined. If n_1 and n_2 are the numbers of atoms of the two species, and $n_1 < n_2$, then energy bounds can be calculated as follows:

$$\text{Lower Bound: } \gamma_{210} = [E_{total} - 2n_1E_{SiC} - (n_2-n_1)E_2]/(2L_xL_y)$$

$$\text{Upper Bound: } \gamma_{210} = [E_{total} - 2n_2E_{SiC} + (n_2-n_1)E_1]/(2L_xL_y)$$

Table 5 shows the results of these simulations, and several notable trends can be observed. The most obvious is that almost all potentials find the two terminating chemistries of the [210] to have roughly the same interfacial energy, with the [310] being equal to these or with slightly lower energetics. Although the energetics of the [210] Σ5 GBs in the DFT simulations performed are also found to be almost identical, these simulations find the [310] GB to have distinctly lower energy. Because all the potentials behaved about the same, the construction of these GBs does not eliminate any one potential from consideration. From a structural perspective, all potentials and DFT found roughly the same structure to be the minimum energy state, allowing for very small variations in position for each potential.

Table 5. Interfacial energies (J/m^2) of Σ5 tilt boundaries produced through the minimization of DFT structures.

Reference	2	5	6	6 REBO	7	10	DFT
[210] C[a]	. . .	. . .	. . .	. . .	. . .	. . .	. . .
Unrelaxed minimization	3.06–3.31	5.81–6.40	3.41–3.91	3.04–3.54	5.58–6.23	2.44–2.92	. . .
DFT minimization	4.22–4.47	5.81–6.40	3.41–3.91	3.04–3.54	5.58–6.23	2.42–2.91	3.62–3.91
[210] Si[b]	. . .	. . .	. . .	. . .	. . .	. . .	. . .
Unrelaxed minimization	4.34–4.59	4.09–4.68	3.40–3.90	3.22–3.72	2.88–3.54	1.88–2.37	
DFT minimization	3.96–4.21	425–4.84	3.00–3.50	3.22–3.72	2.88–3.54	2.50–2.99	3.61–3.92
[310]	. . .	. . .	. . .	. . .	. . .	. . .	. . .
Unrelaxed minimization	2.86	5.28	3.34	3.36	4.53	2.90	. . .
DFT minimization	3.56	4.83	3.19	2.32	2.94	2.58	1.98

[a] C-terminated surface.
[b] Si-terminated surface.

5. Amorphous SiC

Because the a-SiC that forms at SiC-SiC GBs is of great interest in terms of both its energetics and mechanical response, it is worthwhile to determine if and how well each potential can produce these structures. In molecular dynamics, a-SiC can be created by the quenching of liquid SiC. Although variations in the initial temperature of the liquid and cooling rate of the quench will likely create different amorphous structures, much as they would if created experimentally, for this survey of potentials, the a-SiC will be created as follows: a minimized SiC-C3 structure is ramped up to a temperature of 6000 K, over 1 μs, then quenched back to 1 K over

6 ns, and finally the structure is minimized again. Figure 5 shows the difference between a perfect SiC-C3 crystal and a-SiC. This procedure was applied to all potentials still under consideration, thus creating a library of a-SiC samples. To further understand how each potential responds to different amorphous structures, each a-SiC sample is minimized again with each potential, thus creating six samples for each potential. To compare these various samples, however, it is first necessary to describe how a-SiC can be characterized and described.

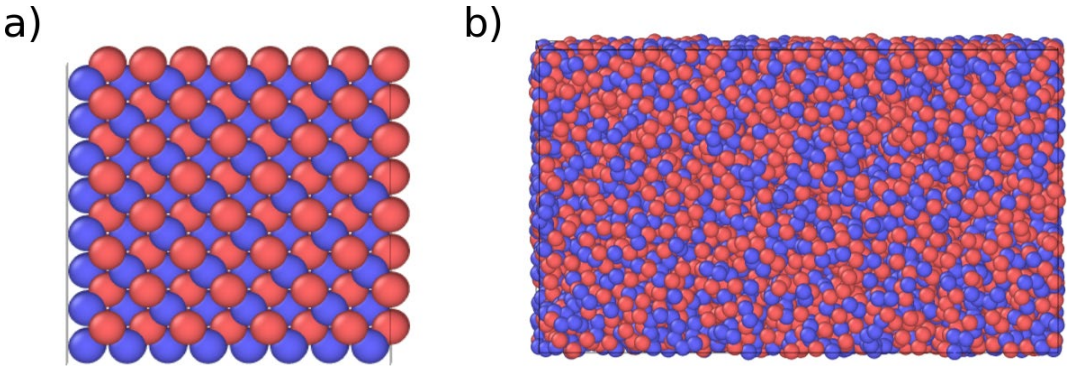

Figure 5. a) SiC-C3 perfect crystal and b) a-SiC sample created through the above-mentioned procedure. Si atoms are shown red and C is shown in blue.

5.1 Characterizing Amorphization

By its nature, an amorphous structure is difficult to characterize. Therefore, it is necessary to find a metric in which to describe a-SiC to allow for comparison between the various structures produced by the potentials as well as with experimental results. In past work on a-SiC,[4] researchers proposed a simple metric to define the degree of disorder in the structure (χ), given by the following equation:

$$\chi = \frac{n_{cc}}{n_{cs}}, \tag{1}$$

where n_{cc} and n_{cs} are the average number of C and Si nearest neighbors, respectively, for a C atom. These values can be determined from the radial distribution function, which is easy to calculate for an atomistic simulation (Figure 6) and can also be found for experimental samples from the electron diffraction intensity profiles. In past studies of a-SiC, researchers have found values of $\chi \approx 0.5$ using atomistics,[4] $\chi \approx 0.6$ using DFT, and $\chi \approx 0.41$ and $\chi \approx 0.47$ determined experimentally by Ishimaru et al.[28] for annealed and irradiated samples, respectively. These experimentally measured, reduced radial, distribution functions find a C-C peak at 1.51 Å (1.47 Å in MD), a significant departure from the C-C peak of 3.06 Å in perfect SiC-C3. This value of 1.51 Å is between the nearest C neighbor in diamond (1.43 Å) and graphite (1.55 Å), highlighting some of the physics behind the amorphization with regards to C bonding. The sum of n_{cc} and

n_{cs} (n_c), which gives the average number of atoms C is bonded to in the sample, can also provide insight into the structure. An n_c value closer to 3 implies a more graphitic-like bonding state for the C, whereas a value closer to 4 implies a more diamond cubic structure to the bonding. These are all quantities that can be determined experimentally, and therefore it may be possible to create simulations in which the amorphization is the same as experimental samples. This also raises the possibility of surveying a range of χ values to suggest degrees of amorphization that might produce inferior or superior mechanical response, allowing for the targeted production of samples.

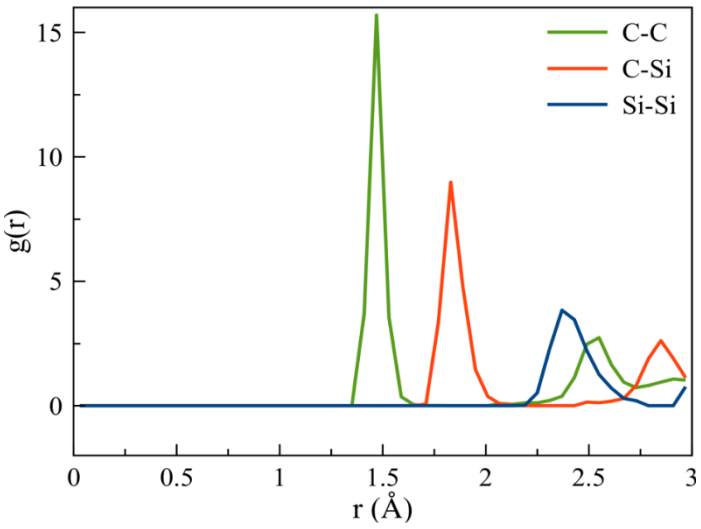

Figure 6. Radial distribution function from an MD sample of a-SiC. For these simulations, it is possible to individually analyze C-C, C-Si, and Si-Si bonding.

5.2 Amorphization Results

Following the procedure discussed above, six a-SiC samples were produced for all six potentials still under consideration. An initial comparison was made between the χ values of each sample for each potential, as well as through plotting χ versus density. From the comparison of amorphization factors (Figure 7a), observed that, except for the a-SiC sample produced using the REBO formulation, the χ values of a given sample are relatively constant regardless of the potential used. This suggests a degree of stability in these structures. The variations in the Erhart and Albe[6] REBO formulation suggest that it may be creating structures that are not well modeled by some of the other potentials. This is highlighted when the density of the samples is considered (Figure 7b), because the samples produced by both formulations of the Erhart and Albe[6] Tersoff potential have significantly lower densities than those produced by the other potentials. This behavior was previously discussed by Pastewka et al.,[11] who noted that these potentials appear to favor a dimerization structure that is somewhat different than those found in experiment.

This suggests that neither formulation of the Erhart and Albe[6] Tersoff potential may be viable to study the amorphization of SiC. Figure 7 also shows that the MEAM potential (Huang et al.[7]) predicts much lower densities than the other potentials for each sample. This, in conjunction with its prediction of n_C values larger than 4 for many of the samples, which is nonphysical because it should lie between 3 and 4, suggests that the MEAM potential also would not be a viable potential for these structures. The amorphization factors of the a-SiC sample produced by the Tersoff[2] potential are notably higher than those found in past studies of a-SiC. Because this potential was able to produce reasonable values for all other samples, it is still a candidate for this study; however, care should be taken because it may be necessary to use an alternate approach to create the amorphous structure if this potential were to be used.

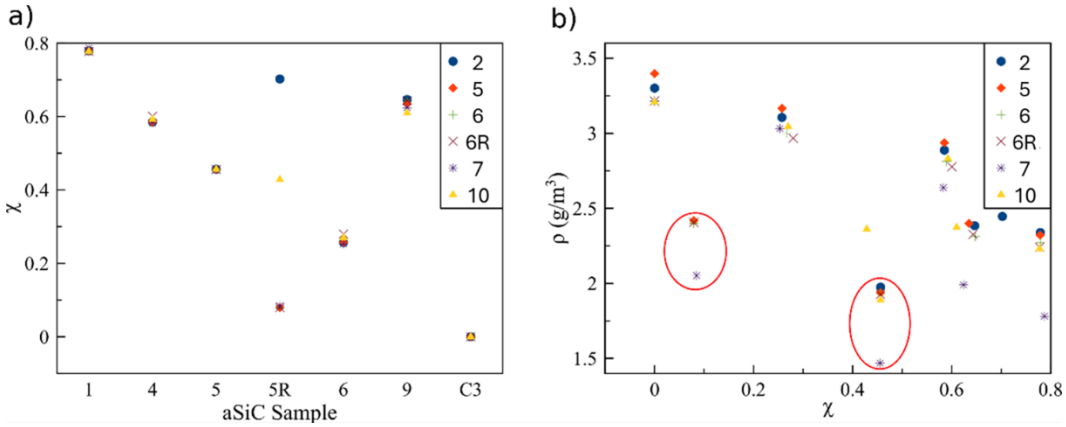

Figure 7. a) Amorphization factor (χ) found for each a-SiC sample for each potential. b) Density as a function of amorphization factor for all potentials. Circled data represent outliers produced by the two formulations of the Erhart and Albe[6] Tersoff potential.

5.3 Effect of Quench Rate

To better analyze the three potentials still under consideration (Tersoff,[2] Devanathan et al.,[5] and Jiang et al.[10]), a more thorough study of a-SiC was conducted in which the quench rate from the liquid SiC is varied. In past work on a-SiC using MD, Xue et al.[29] found this to result in different values of χ, and, as such, their procedure is duplicated, with quench rates ranging from 1×10^{11} to 1×10^{14} K/s considered. To better evaluate each potential individually, only a-SiC structures created by the potential being used were considered, because it is possible that the initial state of the cross-potential results is causing error or bias. For each simulation, elastic constants were determined for the resultant samples, because this may help to gain insight into how the degree of amorphization may influence the mechanical response of the system. Figure 8 shows that the amorphous structure is much more anisotropic than the initial SiC-C3. Although

this is not surprising, it does mean that the determination of the Young's modulus will provide limited information since this value will change with the direction of loading. Therefore, the shear modulus of the system was determined to evaluate the system as a whole.

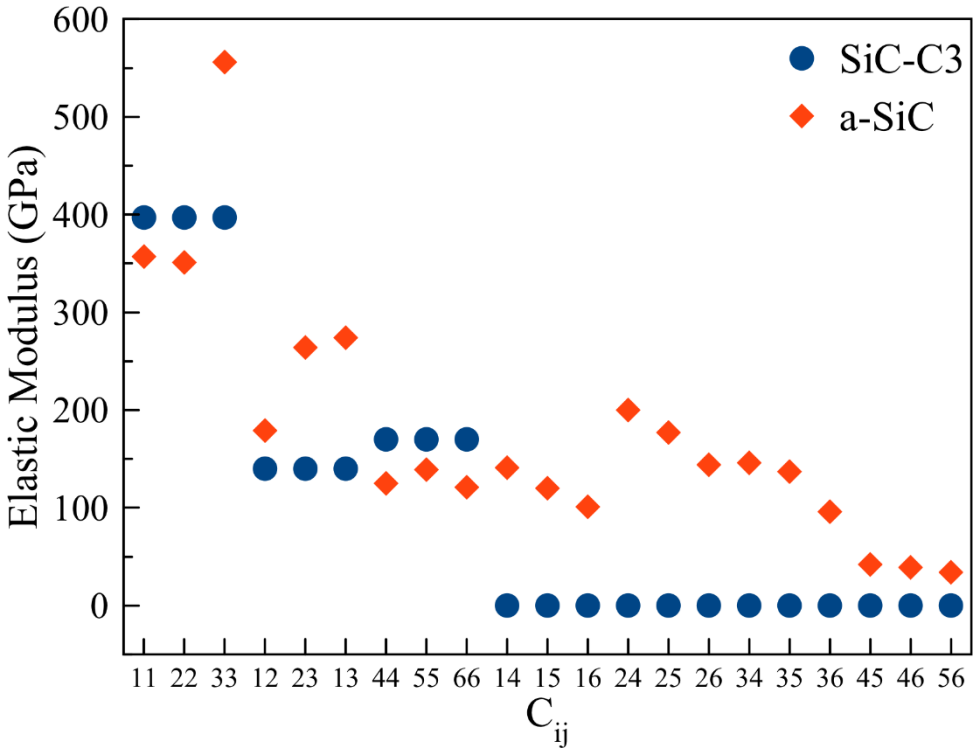

Figure 8. Comparison of elastic constants between bulk SiC-C3 and a-SiC created using EDIP (χ = 0.6).[10]

Figure 9a shows variation in the amorphization factor with quench rate. Although a Tersoff potential (Devanathan et al.[5]) and EDIP (Jiang et al.[10]) behave as expected, becoming less structured as the quench rate is increased, the Tersoff[2] potential has the opposite trend. This nonphysical behavior, in conjunction with amorphization factors larger than 1, suggest this would not be good potential for use on a-SiC. When considering the effect of amorphization on the shear modulus, in previous work, Xue and Niu,[30] who evaluated the response of SiC as it was doped with various amounts of a-SiC, found that the shear modulus would drop precipitously before leveling out at high amorphization factors. As shown in Figure 9b, only EDIP (Jiang et al.[10]) is found to exhibit this behavior, because two Tersoff potentials (Tersoff[2] and Devanathan et al.[5]) have fluctuations in the shear modulus as the amorphization factor increased. For this reason, the Devanathan et al.[5] Tersoff potential is also likely unsuitable for the study of a-SiC.

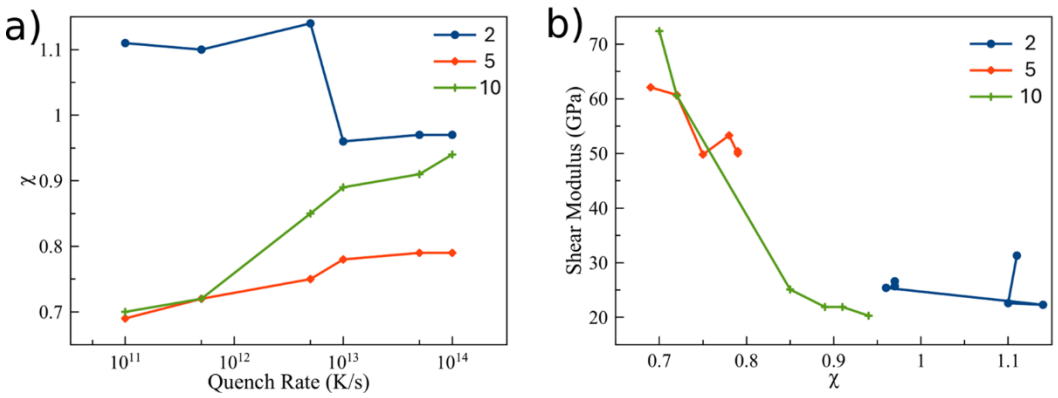

Figure 9. Comparison of elastic constants between bulk SiC-C3 and a-SiC created using EDIP (χ = 0.6).[10]

6. Conclusion

After a complete survey of multiple interatomic potentials for the Si-C system, the EDIP by Jiang et al.[10] is found to be the most suitable for the study of SiC GBs and Si-C composites. However, the Devanathan et al.[5] potential also performed well and does have a lower computational cost, so it could be useful for very large simulations. The Tersoff[2] potential also performed well, except for amorphous SiC. Because this potential also has a REBO variation, which is a better model for strength than conventional potentials, it may be useful for mechanical simulations.

7. References

1. Plimpton S. Fast parallel algorithms for short-range molecular dynamics. Journal of Computational Physics. 1995;117(1):1–19.
2. Tersoff J. Modeling solid-state chemistry: Interatomic potentials for multicomponent systems. Physical Review B. 1989;39(8):5566.
3. Tersoff J. Carbon defects and defect reactions in silicon. Physical Review Letters. 1990;64(15):1757.
4. Tersoff J. Chemical order in amorphous silicon carbide. Physical Review B. 1994;49(23):16349.
5. Devanathan R, Diaz de la Rubia T, Weber WJ. Displacement threshold energies in β-SiC. Journal of Nuclear Materials. 1998;253(1-3):47–52.
6. Erhart P, Albe K. Analytical potential for atomistic simulations of silicon, carbon, and silicon carbide. Physical Review B. 2005;71(3):035211.
7. Huang H, Ghoniem NM, Wong JK, Baskes M. Molecular dynamics determination of defect energetics in β-SiC using three representative empirical potentials. Modelling and Simulation in Materials Science and Engineering. 1995;3(5):615.
8. Gao F, Weber WJ. Empirical potential approach for defect properties in 3C-SiC. Nuclear Instruments and Methods in Physics Research Section B: Beam Interactions with Materials and Atoms. 2002;191(1-4):504–508.
9. Belko V, Posselt M, Chagarov E. Improvement of the repulsive part of the classical interatomic potential for SiC. Nuclear Instruments and Methods in Physics Research Section B: Beam Interactions with Materials and Atoms. 2003;202:18–23.
10. Jiang C, Morgan D, Szlufarska I. Carbon tri-interstitial defect: a model for the D II center. Physical Review B. 2012;86(14):144118.
11. Pastewka L, Klemenz A, Gumbsch P, Moseler M. Screened empirical bond-order potentials for Si-C. Physical Review B. 2013;87(20):205410.
12. Vashishta P, Kalia RK, Nakano A, and Rino JP. Interaction potential for silicon carbide: a molecular dynamics study of elastic constants and vibrational density of states for crystalline and amorphous silicon carbide. Journal of Applied Physics. 2007;101(10):103515.

13. Lambrecht WRL, Segall B, Methfessel M, Van Schilfgaarde M. Calculated elastic constants and deformation potentials of cubic SiC. Physical Review B. 1991;44(8):3685.

14. Kamitani K et al. The elastic constants of silicon carbide: a Brillouin-scattering study of 4H and 6H SiC single crystals. Journal of Applied Physics. 1997;82(6):3152–3154.

15. Harris GL. Properties of silicon carbide. Number 13. Iet, 1995.

16. Klemens PG, Neuer G, Sundqvist B, Uher C, White GK. Numerical data and functional relationships in science and technology. Vol. 15c. Springer; 1991.

17. Brewer L. The cohesive energies of the elements. Lawrence Berkley National Laboratory (US); 1977. https://escholarship.org/uc/item/08p2578m

18. Jung SC, Han Y-K. Facet-dependent lithium intercalation into Si crystals: Si (100) vs. Si (111). Physical Chemistry Chemical Physics. 2011;13(48):21282–21287.

19. Jaccodine RJ. Surface energy of germanium and silicon. Journal of the Electrochemical Society. 1963;110(6):524–527.

20. Ramaseshan S. The cleavage properties of diamond. Proceedings of the Indian Academy of Sciences- Section A, volume 24. New Delhi, India. Springer; c1946. p. 114.

21. Powers JM, Wander A, Van Hove MA, Somorjai GA. Structural analysis of the β-SiC (100)-(2 × 1) surface reconstruction by automated tensor LEED. Surface Science. 1992;260(1-3):L7–L10.

22. Glass CW, Oganov AR, Hansen N. USPEX–evolutionary crystal structure prediction. Computer Physics Communications. 2006;175(11-12):713–720.

23. Bean AR, Newman RC. The solubility of carbon in pulled silicon crystals. Journal of Physics and Chemistry of Solids. 1971;32(6):1211–1219.

24. Gao F, Bylaska EJ, Weber WJ, Corrales LR. Native defect properties in β-SiC: ab initio and empirical potential calculations. Nuclear Instruments and Methods in Physics Research Section B: Beam Interactions with Materials and Atoms. 2001;180(1-4):286–292.

25. Watanabe H, Yamada N, Okaji M. Linear thermal expansion coefficient of silicon from 293 to 1000 K. International Journal of Thermophysics. 2004;25(1):221–236.

26. Stoupin S, Shvyd′ko YV. Ultraprecise studies of the thermal expansion coefficient of diamond using backscattering X-ray diffraction. Physical Review B. 2011;83(10):104102.

27. Li Z, Bradt RC. Thermal expansion of the cubic (3C) polytype of SiC. Journal of Materials Science. 1986;21(12):4366–4368.

28. Ishimaru M, Bae I-T, Hirotsu Y, Matsumura S, Sickafus KE. Structural relaxation of amorphous silicon carbide. Physical Review Letters. 2002;89(5):055502.

29. Xue K, Niu L-S, Shi H-J. Effects of quench rates on the short- and medium-range orders of amorphous silicon carbide: a molecular-dynamics study. Journal of Applied Physics. 2008;104(5):053518.

30. Xue K, Niu L-S. Understanding the changes in mechanical properties due to the crystalline- to-amorphization transition in sic. Journal of Applied Physics. 2009;106(8):083505.

List of Symbols, Abbreviations, and Acronyms

a-SiC	amorphous silicon carbide (structure)
DFT	density functional theory
EDIP	environment-dependent interatomic potential
GB	grain boundary
GW	Gao–Weber
LAMMPS	Large-scale Atomic/Molecular Massively Parallel Simulator
MD	molecular dynamics
MEAM	modified embedded-atom method
REBO	reactive empirical bond order
SiC	silicon carbide
Si-C	silicon-carbon

1 (PDF)	DEFENSE TECHNICAL INFORMATION CTR DTIC OCA
1 (PDF)	DEVCOM ARL FCDD RLB CI TECH LIB